
Proceedings Paper:
Biga, V. and Coca, D. orcid.org/0000-0003-2878-2422 (2017) Information-theoretic active contour model for microscopy image segmentation using texture. In: Bracciali, A., Caravagna, G., Gilbert, D. and Tagliaferri, R., (eds.) Computational Intelligence Methods for Bioinformatics and Biostatistics. 13th International Meeting, CIBB 2016, 01-03 Sep 2016, Stirling, UK. Lecture Notes in Computer Science, 10477 . Springer, Cham , pp. 12-26. ISBN 9783319678337

https://doi.org/10.1007/978-3-319-67834-4_2

INFORMATION-THEORETIC ACTIVE CONTOUR MODEL FOR MICROSCOPY IMAGE SEGMENTATION USING TEXTURE

Veronica Biga[1,2], Daniel Coca[2]

(1)The University of Manchester, Faculty of Life Sciences, Oxford Road M13 9PL, veronica.biga@manchester.ac.uk (2)The University of Sheffield, Automatic Control and Systems Engineering Department, Mappin Street S1 3JD, d.coca@sheffield.ac.uk

Keywords: image segmentation, geometric active contour, feature selection, Cauchy-Schwartz distance, Gabor energy

Abstract. High throughput technologies have increased the need for automated image analysis in a wide variety of microscopy techniques. Geometric active contour models provide a solution to automated image segmentation by incorporating statistical information in the detection of object boundaries. Information theoretic measures such as entropy and Kullback-Leibler divergence involve numerical evaluation of ratio-type quantities susceptible to numerical instability, however product-type information theoretic measures, such as the Cauchy-Schwartz distance performing better when the size of the feature space shrinks [1]. Using accurate shape derivation techniques [2], a new geometric active contour model for image segmentation is defined combining Cauchy-Schwartz distance and Gabor energy texture filters. The performance is demonstrated on images from the Brodatz dataset and phase-contrast microscopy images of human embryonic carcinoma cells.

1 Scientific Background

Due to high throughput technology, a great influx of imaging data has become available in biomedical research producing large datasets that need to be processed in a reliable and unbiased way. As a result, there is an increased need for computer automation throughout the imaging framework [3]. Existing work is focused either on pre-processing the image to remove artifacts and enhance signal-to-noise ratio [4]; or using local intensity and/or texture information to delineate the cell surface from the background [5]. The latter cattegory is non technology-specific and coupled with the ability to estimate parameters from data has the potential to unify different detection techniques [6].

Image segmentation is the task of partitioning an image into meaningful regions such as objects and the background. Region-based segmentation takes into account the statistical properties of the image for example through density estimation techniques. The aim of unsupervised segmentation is to partition the image into regions with most distinct statistical properties. Often the target regions are not easily characterized by Gaussian-distributed pixel intensities making the detection by standard image analysis techniques (thresholding, edge-detection, region-based and connectivity preserving techniques) extremely challenging. This is the case in phase-contrast microscopy which is a widely used imaging technology, however images produced have low signal-to-noise ratio and illumination artifacts (bright halo around boundaries) caused by changes in object shape [4].

In this study, the Cauchy-Schwartz measure [1] of divergence is used to optimise image segmentation. Product-type measures such as Cauchy-Schwartz distance and Battacharyya distance [7] have numerical advantages over ratio-type measures including

Kullback-Leibler [8] and Renyi's entropy in the approximation of region-specific distributions. By combining information theory with Gabor energy texture descriptors and a supervised feature selection strategy, an automated segmentation strategy is described that can recover boundaries in test images and challenging phase-contrast microscopy examples.

2 Materials and Methods

The partitioning of image Ω_0 into two non-overlapping regions: the *target* region Ω and the *background* region $\Omega_0 \setminus \Omega$ is defined by function $\mathbf{f} : \Omega_0 \subset \mathbb{R}^2 \rightarrow \mathbb{R}^n, \mathbf{f}(\mathbf{x}) = [f_1(\mathbf{x}), f_2(\mathbf{x}), ..., f_n(\mathbf{x})]^T$ which associates any image location $\mathbf{x} = (x, y) \in \mathbb{R}^2$ to a vector of features f_i. The dimension of the feature space is determined by the nature of features,e.g. n=1 for grayscale intensity, n=3 for color images or large n in the case of texture. Features observed over the target and background regions represent random variables independently sampled from a target distribution, $p_t(\mathbf{f}(\mathbf{x})) = \frac{1}{||\Omega||}\int_{\Omega} K(\mathbf{f}(\mathbf{x}) - \mathbf{f}(\hat{\mathbf{x}}))d\hat{\mathbf{x}}$ and a background distribution, $p_b(\mathbf{f}(\mathbf{x})) = \frac{1}{||\Omega_0 \setminus \Omega||}\int_{\Omega_0 \setminus \Omega} K(\mathbf{f}(\mathbf{x}) - \mathbf{f}(\hat{\mathbf{x}}))d\hat{\mathbf{x}}$ where $\hat{\mathbf{x}}$ denote uniformly distributed sampling locations from where the feature observations $\mathbf{f}(\hat{\mathbf{x}})$ are collected and the density estimation kernel is a Gaussian:

$$K(\mathbf{f}(\mathbf{x})) = \frac{1}{(2\pi)^{n/2}\text{det}(\Sigma)^{1/2}} \exp\left(-\frac{1}{2}\mathbf{f}(\mathbf{x})^T\Sigma^{-1}\mathbf{f}(\mathbf{x})\right), \Sigma = \sigma^2\mathbf{I} \ . \tag{1}$$

In the following, the use of the Cauchy-Schwartz (CS) information-theoretic measure is discussed as basis for defining a new image segmentation model. The assumption is that given a partitioning of the image, region-specific p_t and p_b can be optimally estimated by modifying the partitioning in the direction of maximising CS distance:

$$D_{CS}\left(p_t(\mathbf{f}(\mathbf{x})), p_b(\mathbf{f}(\mathbf{x}))\right) = -\log \frac{\int_{\mathbb{R}^n} p_t(\mathbf{f}(\mathbf{x}))p_b(\mathbf{f}(\mathbf{x}))d\mathbf{f}}{\sqrt{\int_{\mathbb{R}^n} p_b^2(\mathbf{f}(\mathbf{x}))d\mathbf{f}\int_{\mathbb{R}^n} p_t^2(\mathbf{f}(\mathbf{x}))d\mathbf{f}}} \geq 0 \ . \tag{2}$$

Geometric active contour model based on information theory. The active contour partitioning of the image is represented using a level set function $\Phi(\mathbf{x}) \geq 0, \mathbf{x} \in \Omega; \Phi(\mathbf{x}) \leq 0, \mathbf{x} \in \Omega_0 \setminus \Omega; \Phi(\mathbf{x}) = 0, \mathbf{x} \in \partial\Omega$. The region-based geometric active contour model based on CS distance is defined as:

$$J(\Phi) = \int_{\mathbb{R}^n} \frac{p_t(\mathbf{f}(\mathbf{x}))p_b(\mathbf{f}(\mathbf{x}))}{\sqrt{\int_{\mathbb{R}^n} p_t^2(\mathbf{f}(\mathbf{x}))d\mathbf{f}\int_{\mathbb{R}^n} p_b^2(\mathbf{f}(\mathbf{x}))d\mathbf{f}}}d\mathbf{f} + \mu\int_{\partial\Omega} ds = J_1(\Phi) + J_2(\Phi) \tag{3}$$

where $J_1(\Phi)$ represents the argument of the logarithm in (2) and $J_2(\Phi)$ imposes minimum length of the contour. The evolution of $\Phi(\mathbf{f}(\mathbf{x}), t)$ from an initial given state $\Phi(\mathbf{f}(\mathbf{x}), 0) = \Phi_0(\mathbf{f}(\mathbf{x}))$ in the direction of minimising (3) is parametrised by $t \geq 0$.

The term $J_1(\Phi) = \int_{R^n} k(\mathbf{x}, \Omega)d\mathbf{f}$ is described as a region-based term with region-dependent descriptor $k(\mathbf{x}, \Omega) = G_1(\mathbf{x}, \Omega)G_2(\mathbf{x}, \Omega)G_3(\mathbf{x}, \Omega)^{-1/2}G_4(\mathbf{x}, \Omega)^{-1/2}$ in the sense of shape derivation theory [10], whereby:

$$\begin{aligned} G_1(\mathbf{x}, \Omega) &= p_t(\mathbf{f}(\mathbf{x})); \quad G_3(\mathbf{x}, \Omega) = \int_{R^n} p_t^2(\mathbf{f}(\mathbf{x}))d\mathbf{f}; \\ G_2(\mathbf{x}, \Omega) &= p_b(\mathbf{f}(\mathbf{x})); \quad G_4(\mathbf{x}, \Omega) = \int_{R^n} p_b^2(\mathbf{f}(\mathbf{x}))d\mathbf{f}; \end{aligned} \tag{4}$$

Therefore, the Euler derivative of J_1 in the direction of $\mathbf{v}$ is:

$$\begin{aligned} dJ_{1r}(\Omega, \mathbf{v}) = &-\frac{A(\mathbf{x}, \Omega)}{||\Omega||}\int_{\partial\Omega}\left(1 - \frac{G_1(\mathbf{x}, \Omega)}{G_3(\mathbf{x}, \Omega)}\right)G_2(\mathbf{x}, \Omega) * K(\mathbf{f}(\mathbf{x}))\,(\mathbf{v}\cdot\mathbf{n})\,ds + \\ &+\frac{A(\mathbf{x}, \Omega)}{||\Omega_0 \setminus \Omega||}\int_{\partial\Omega}\left(1 - \frac{G_2(\mathbf{x}, \Omega)}{G_4(\mathbf{x}, \Omega)}\right)G_1(\mathbf{x}, \Omega) * K(\mathbf{f}(\mathbf{x}))\,(\mathbf{v}\cdot\mathbf{n})\,ds \end{aligned} \tag{5}$$

where $A(\mathbf{x},\Omega) = G_3^{-1/2}(\mathbf{x},\Omega)G_4^{-1/2}(\mathbf{x},\Omega)$ and the operator $*$ denotes convolution. The term $J_2(\Phi)$ is a boundary-based term with boundary-independent descriptor, therefore $dJ_{2r}(\Omega,\mathbf{v}) = -\int_{\partial\Omega}\mu\kappa(\mathbf{v}\cdot\mathbf{n})ds$. The evolution equation for the geometric active contour becomes:

$$\begin{aligned}\frac{\partial\Phi}{\partial t} &= \Big[\frac{A(\mathbf{x},\Omega)}{||\Omega||}\left(1-\frac{G_1(\mathbf{x},\Omega)}{G_3(\mathbf{x},\Omega)}\right)(G_2(\mathbf{x},\Omega)*K(\mathbf{f}(\mathbf{x}))) - \\ &- \frac{A(\mathbf{x},\Omega)}{||\Omega_0\setminus\Omega||}\left(1-\frac{G_2(\mathbf{x},\Omega)}{G_4(\mathbf{x},\Omega)}\right)(G_1(\mathbf{x},\Omega)*K(\mathbf{f}(\mathbf{x}))) + \mu\text{div}\left(\frac{|\nabla\Phi|}{||\nabla\Phi||}\right)\Big]\mathbf{n}\ .\end{aligned} \tag{6}$$

Gabor energy-based texture features. Texture features include spatial information of pixel intensities. Commonly used in image processing is Gabor filtering which decomposes the image into sub-bands with a preferred orientation and spatial frequency by kernel convolution. The use of Gabor energy features sets the basis for a nonlinear multi-scale method of describing texture that resembles the way information is interpreted in the visual cortex, [9]. A 2D Gabor filter centred in (x_0,y_0) is $x\prime = (x-x_0)\cos\theta + (y-y_0)\sin\theta$, $y\prime = -(x-x_0)\sin\theta + (y-y_0)\cos\theta$:

$$g_{\lambda,\sigma,\gamma,\theta,\varphi}(x,y) = e^{-\frac{x\prime^2+\gamma^2y\prime^2}{2\sigma^2}}\cos\left(2\pi\frac{x\prime}{\lambda}+\varphi\right) \tag{7}$$

where $\theta\in[0\ \pi)$ is the rotation angle of the gaussian envelope and λ and $\varphi\in(-\pi\ \pi]$ denote the spatial frequency and phase of the sinusoidal carrier. The Gaussian envelope is characterised by parameters γ, which specifies ellipticity and σ, a scaling parameter which controls the size of the Gaussian. The ratio σ/λ controls the number of parallel on and off stripes that the kernel contains. This ratio is determined by the bandwidth b, $\frac{\sigma}{\lambda} = \frac{1}{\pi}\sqrt{\frac{\ln 2}{2}}\frac{2^b+1}{2^b-1}$. The response of a Gabor filter (7) applied to an image is:

$$r_{\lambda,\sigma,\gamma,\theta,\varphi} = \int_\Omega I(u,v)g_{\lambda,\sigma,\gamma,\theta,\varphi}(x-u,y-v)dudv\ . \tag{8}$$

Gabor energy represents the combined magnitude of two phase-shifted responses:

$$e_{\lambda,\sigma,\gamma,\theta}(x,y) = \sqrt{r^2_{\lambda,\sigma,\gamma,\theta,0}(x,y) + r^2_{\lambda,\sigma,\gamma,\theta,-\frac{\pi}{2}}(x,y)}\ . \tag{9}$$

Single orientation texture features. Gabor energy feature function can be defined by discretising $\lambda = [\lambda_{min}, \lambda_{min}+\Delta\lambda,\dots]$, $\gamma = [\gamma_{min},\gamma_{min}+\Delta\gamma,\dots]$ and $\theta = [\theta_1,\theta_2,\dots], \theta_k = k\frac{\pi}{N}, k = \overline{0,N-1}$. We consider the case of $b=1$. Multiple single features $\mathbf{f}^1_{n,k} = e_{\lambda_n,\gamma_n,\theta_k}(x,y)$ are ombined into a set:

$$\mathbf{f}^1 : \Omega_0\in\mathbb{R}^n, \mathbf{f}^1(x,y) = [\mathbf{f}^1_{1,0}(x,y), \mathbf{f}^1_{1,1}(x,y)\dots\mathbf{f}^1_{n,N-1}(x,y)]^T; \tag{10}$$

Combined orientation texture features. For textures without a preferred spatial orientation, a combined Gabor energy feature representing the superposition of energies $\mathbf{f}^2_n(x,y) = \sum_{k=1}^N e_{\lambda_n,\gamma_n,\theta_k}(x,y)$ for all θ is defined as a feature set:

$$\mathbf{f}^2 : \Omega_0\in\mathbb{R}^n, \mathbf{f}^2(x,y) = [\mathbf{f}^2_1(x,y),\dots\mathbf{f}^2_n(x,y)]^T \tag{11}$$

Feature selection strategy. At iteration time $t=0$, consider a complete set of features was generated in $\mathbf{f}_{pool,t} = [\mathbf{f}_{pool,t,1}(x,y), \mathbf{f}_{pool,t,2}(x,y),\dots]$. The supervised feature selection strategy involves starting with only one feature in the selected set $\mathbf{f}_{sel,0}(x,y) = \mathbf{f}_{pool,t,1}(x,y)$ and a testing set $\mathbf{F} = [\mathbf{f}_{sel,t}]$. The first feature, $\mathbf{f}_{pool,t,1}(x,y)$, is chosen as the

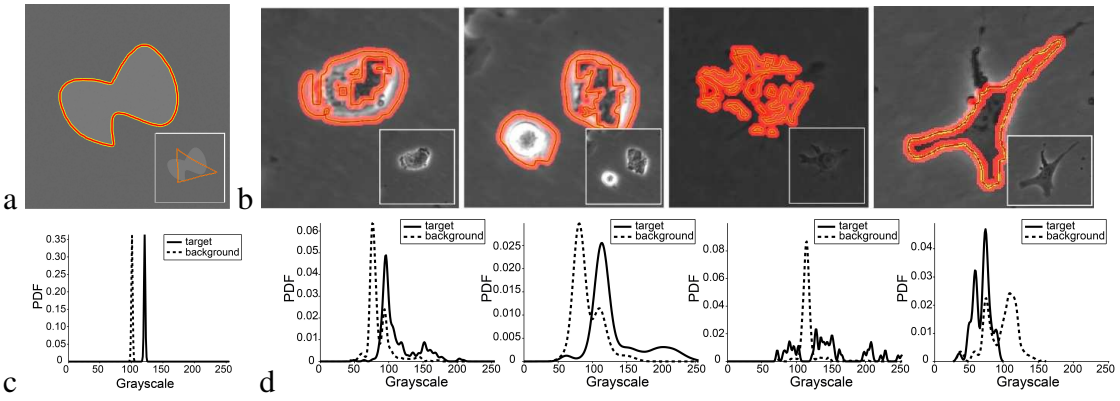

Figure 1: Grayscale-intensity based segmentation using CS model: recovered contour in (a) artificial image and (b) phase-contrast microscopy images of cells; corresponding target and background distributions at final iteration shown in panels (c) and (d) respectively. Parameters $\mu = 0.01; w = 15$ and $\mu = 0.2; w = 5$ in (a) and (b) respectively.

minimisation of $CS_0(p_t, p_b)$ evaluated according to a three step **Optimisation:** (i) for the feature set **F**, find optimal bandwidth σ_t;(ii) for the partitioning $\Phi = \Phi_t$ and given F, σ_t estimate p_t, p_b ; (iii) using $p_t,\ p_b$ update $CS_u(p_t, p_b)$.

Step 1. for $\mathbf{F} = \mathbf{f}_{sel,t}$, calculate $CS_u(p_t, p_b)$ with **Optimisation**; **Step 2.** increase iteration count $t = t+1$; **Step 3.** from all remaining features in $\mathbf{f}_{pool,t-1}$ consider the temporary selection $\mathbf{f}_{temp,t} = [\mathbf{f}_{sel,t}\mathbf{f}_{pool,t,k}, \forall k]$ and calculate for each k the value of $CS_u(p_t, p_b)$ when $\mathbf{F} = \mathbf{f}_{temp,t}$ with **Optimisation**; **Step 4.** choose $\mathbf{f}_{pool,t,k}$ that generates the largest decrease in the criterion and generate new $\mathbf{f}_{sel,t} = [\mathbf{f}_{sel,t}, \mathbf{f}_{pool,t,k}]$ **Step 5.** return to **Step 1**. The feature selection strategy terminates for $CS_t(p_t, p_b) < 0.1CS_0(p_t, p_b)$.

Numerical implementation. The level set function Φ is initialised as a signed distance function and the pixels in the narrow-band region around the contour are updated followed by reinitialisation of the distance function to prevent numerical errors.The optimal variance in each dimension is computed with Scott's rule $\sigma^2_{\mathbf{X}} = \frac{1}{n}\sum_{i=1}^{n}\sigma^2_{ii}; \sigma^\star = \sigma_{\mathbf{X}} m^{\frac{1}{n+4}}$. The Parzen density estimation kernel is $K_{\sigma^\star}(z) = \frac{1}{\sqrt{2\pi}\sigma^\star}\exp^{-\frac{z^T z}{2\sigma^{\star 2}}}$.The time step is limited to $\Delta t = 0.45(2\frac{max(|F^u|)}{h} + 2\frac{\mu}{h} + 2\frac{\mu}{h^2})^{-1}$.The main parameters reported are stiffness $\mu \in [0, 1]$ and width of the narrow band w.

3 Results

Segmentation of phase-contrast images based on grayscale intensity only partially recovers boundaries.The CS-based geometric active contour was evaluated on a test image and real microscopy images of cells acquired with a phase-contrast microscope (Figure1). Boundaries of the test image were recovered despite similar mean intensity of target and background. However, the microscopy images contain target regions with significant overlap to the background and boundaries are only partly recovered. Further halo artifacts and the inclusion of dark and bright objects raise the biggest problems resembling thresholding techniques. These examples indicate that microscopy images cannot be segmented using grayscale intensity alone and further information is hidden in the texture characteristics of both regions.

Gabor features enable detection of noisy object boundaries in textured images. To investigate the ability to recover boundaries using Gabor texture features, test images were generated by fusing samples from the Brodatz [1] dataset (Figure 2). The fused textures have similar mean intensity and noisy illumination which resemble properties of microscopy images. A single orientation feature space was generated using $b = 1$,

[1] http://www.ux.uis.no/ tranden/brodatz.html

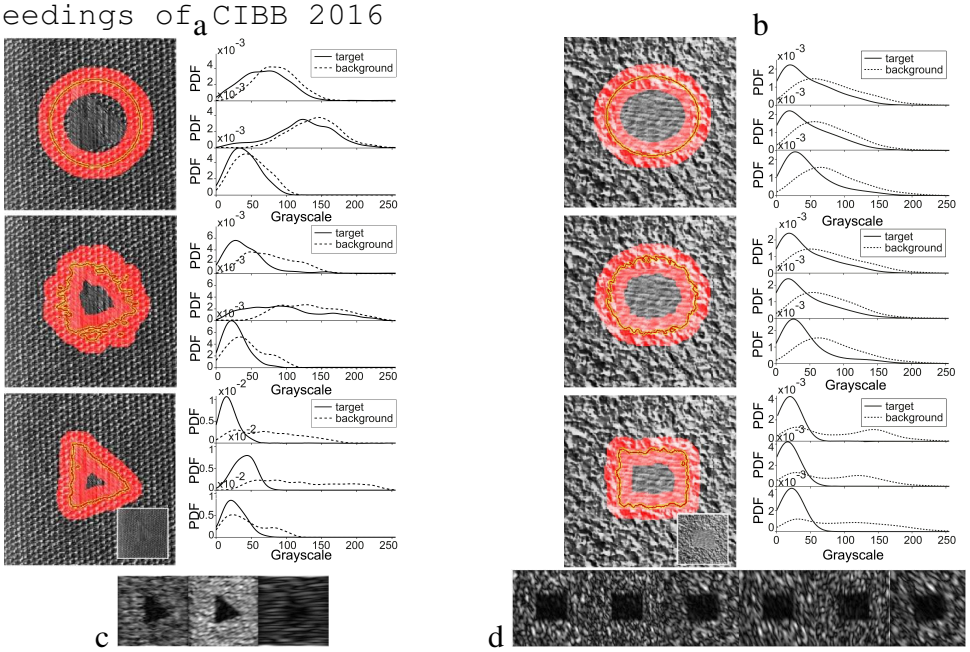

Figure 2: Brodatz texture segmentation examples in images generated as fusion of two textures: (a,b) active contours evolving from initialisation (top) towards final iteration (bottom) and corresponding shape of target and background distributions for the three dominant features from optimal sets showed in (c) and (d) respectively. Parameters $\mu = 0.2,\ w = 15$.

$\lambda = [1/15,\ 1/30,\ 1/60,\ 1/120,\ 1/240]$, $\gamma = [0.2,\ 0.4,\ 0.6,\ 0.8,\ 1]$; this was reduced to an optimal feature set using the CS-based feature selection strategy and the active contour was able to succesfully recover the boundaries despite thetarget and background distributions retaining overlap. The number of selected features is larger in the example (Figure 2b) compared to (Figure 2a) and the selected features are similar highlighting that a sparse feature set improves convergence speed at no cost to the final result.

Cauchy-Schwartz model detects cells in phase-contrast images using Gabor features. The performance of the geometric active contour and feature selection strategy were tested on real microscopy images displaying cells with bright and dark cell interior (Figure 3). The texture of cells has no preffered orientation, therefore the feature space was combined from features at 8 different orientations followed by reduction to an optimal feature set. The active contour was tested on the dark and bright cell on their own and finally on both. In all cases boundaries were correctly detected using few features. As expected, initial CS level exceeds the threshold indicated by the feature selections trategy but falls under at large iteration numbers (Figure 3). The CS trends indicate that the boundaries of the dark cell are detected fastest (Figure 3a) while the combined bright and dark cell segmentation is the slowest (Figure 3c).

4 Conclusions

The challenges of segmentation in phase-contrast microscopy images were addressed through a strategy combining information-theory and Gabor energy features. A new image segmentation model was defined to optimise Cauchy-Schwartz distance between a desired (target) region and the background using a geometric active contour. The model incorporated the use of a product-type measure of divergence and shape derivation techniques known to improve robustness and numerical accuracy. Texture information based on Gabor energy was found to be essential in recovering boundaries of cells of various grayscale intensities. The introduction of texture information posed the problem of increased computational complexity which was solved through a feature selection strategy using the same criterion as the active contour. Performance of texure-based segmentation was demonstrated using single orientation features in textured images adapted from the Brodatz dataset and combined orientation features for miscroscopy images.

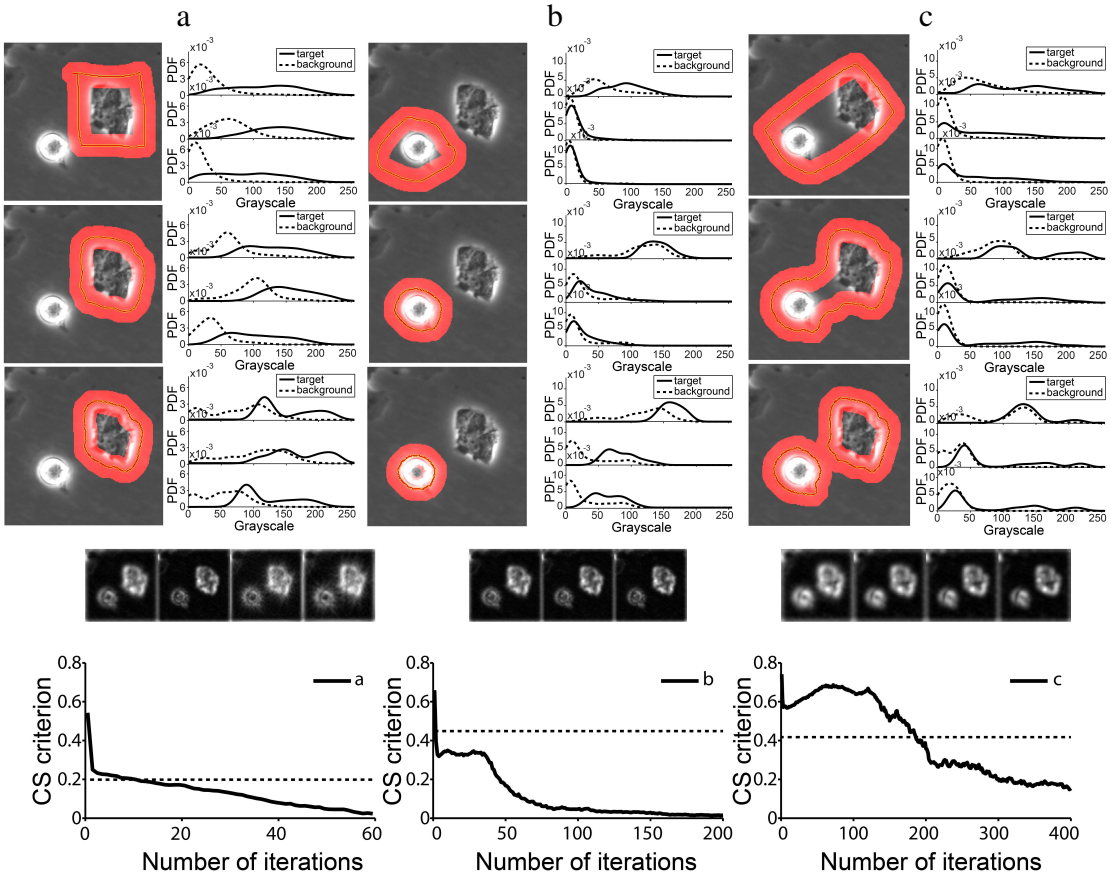

Figure 3: Selective segmentation of cells in phase-contrast microscopy image using texture: (a-c) active contours evolving from initialisation (panel top) towards final interation (panel bottom) applied to a cell with (a) dark, (b) bright and (c) combined grayscale intensity; optimal feature sets and CS values corresponding to (a-c); dashed line indicates optimal values of criterion predicted by the feature selection strategy. Parameters $\mu = 0.2; w = 15$

Acknowledgments

This work was funded by a doctoral research scholarship from The University of Sheffield. Authors kindly thank members of the PW Andrews Laboratory at Centre for Stem Cell Biology for providing the microscopy images of cells.

References

[1] E. Gokcay, J.C.Principe. "Information theoretic clustering". *IEEE Trans Pattern Anal Mach Intell*, vol. 24, no. 2, pp. 158-171, 2002.

[2] S. Jehan-Besson, M. Barlaud, G. Aubert. "Video object segmentation using Eulerian region-based active contours".*Intl Conf Comp Vis*, pp. 353-361, 2001.

[3] K.W. Eliceiri, M.R. Berthold, I.G. Goldberg et al. "Biological imaging software tools". *Nat Meth*, vol. 9, no. 7, pp. 697-710, 2012.

[4] Z. Yin, T. Kanade, D. Xu, J. Fisher. "Understanding the phase contrast optics to restore artifact-free microscopy images for segmentation". *Med Image Anal*, vol. 16, no. 5, pp. 1047-1062, 2012.

[5] M.A. Dewan, M. O. Ahmad, M.N. Swamy. "A method for automatic segmentation of nuclei in phase-contrast images based on intensity, convexitty and texture". *IEEE Trans Biomed Circ Syst*, vol. 8, no. 5, pp. 716-728, 2014.

[6] C. Held, R. Palmisano, L. Haberle et al. "Comparison of parameter-adapted segmentation methods for fluorescence micrographs". *Cytom Part A*, vol. 79, no. 11, pp. 933-945, 2011.

[7] O.V. Michailovich, Y. Rathi, A. Tannenbaum. "Image segmentation using active contours driven by the Battacharya gradient flow". *IEEE Trans on Image Proc*, vol. 16, no. 11, pp. 2787-2801, 2007.

[8] N. Houhou, J.P. Thiran, X. Bresson. "Fast texture segmentation model based on the shape operator and active contour". *Proceedings of IEEE Comp Vis and Pattern Recog*, vol. 53, pp. 1-8, 2008.

[9] N. Petkov, P. Kruizinga. "Computational models of visual neurons specialised in the detection of periodic and aperiodic visual stimuli: Bar and grating cells". *Biol Cybern*, vol. 76, no. 2, pp. 83-96, 1997.

[10] G. Aubert, M. Barlaud, O. Faugeras et al. "Image Segmentation using active contours: Calculus of variations or shape gradients". *SIAM J Appl Math*, vol. 63, pp. 2128-2154, 2002.